Exfoliated Nanosheet Crystallite of Cesium Tungstate with 2D Pyrochlore Structure: Synthesis, Characterization, and Photochromic Properties

Katsutoshi Fukuda,[†] Kosho Akatsuka,[†,‡] Yasuo Ebina,[†] Renzhi Ma,[†] Kazunori Takada,[†] Izumi Nakai,[§] and Takayoshi Sasaki[†,‡,*]

[†]International Center for Materials Nanoarchitectonics and Nanoscale Materials Center, National Institute for Materials Science, 1-1 Namiki, Tsukuba, Ibaraki 305-0044, Japan, [‡]Graduate School of Pure and Applied Sciences, University of Tsukuba, 1-1-1 Tennodai, Tsukuba 305-8571, Japan, and [§]Department of Applied Chemistry, Tokyo University of Science, 1-3 Kagurazaka, Shinjuku, Tokyo 162-8601, Japan

ABSTRACT Layered cesium tungstate, $Cs_{6+x}W_{11}O_{36}$, with two-dimensional (2D) pyrochlore structure was exfoliated into colloidal unilamellar sheets through a soft-chemical process. Interlayer Cs ions were replaced with protons by acid exchange, and quaternary ammonium ions were subsequently intercalated under optimized conditions. X-ray diffraction (XRD) measurements on gluelike sediment recovered from the colloidal suspension by centrifugation showed a broad pattern of a pronounced wavy profile, which closely matched the square of calculated structure factor for the single host layer. This indicates the total delamination of the layered tungstate into nanosheets of $Cs_4W_{11}O_{36}^{2-}$. Microscopic observations by transmission electron microscopy and atomic force microscopy clearly revealed the formation of unilamellar crystallites with a very high 2D anisotropy, a thickness of only ~2 nm *versus* lateral size up to several micrometers. In-plane XRD analysis confirmed that the 2D pyrochlore structure was retained. The colloidal cesium tungstate nanosheet showed strong absorption of UV light with sharp onset, suggesting a semiconducting nature. Analysis of the absorption profile provided 3.6 eV as indirect band gap energy, which is 0.8 eV larger than that of the bulk layered precursor, probably due to size quantization. The nanosheet exhibited highly efficient photochromic properties, showing reversible color change upon UV irradiation.

KEYWORDS: nanosheet · nanomesh · tungsten oxide · self-assembly · photochromism · chromogenic nanomaterial

Nanosheet crystallites obtained through delamination of various layered compounds including clays,[1,2] sulfides,[3–5] oxides,[6–20] and hydroxides[21–24] are attracting intensive research as a new class of nanoscale materials, exhibiting distinctive physicochemical properties associated with dimensions in the nanometer range. Due to the recent emergence of functional nanosheets such as titanium,[6–9] niobium,[10–14] and tantalum[15–17] oxide-related crystallites, their importance is increasingly recognized in the field of material science. These nanosheet crystallites possess high two-dimensional (2D) anisotropy and, therefore, can be regarded as unique inorganic 2D macromolecules having functionalities inherited from the layered parent compounds. Thanks to their polyelectrolytic nature, they can be employed as a building block for electrostatic layer-by-layer self-assembly utilizing oppositely charged polymers,[25–27] nanoparticles,[28] and nanosheets,[29] which allows the well-controlled design of nanostructured materials. Sophisticated functions can be expected through the selection and precisely controlled organization of the components.

Over the past few decades, a series of tungsten oxides have been extensively investigated as an attractive functional material with a number of interesting properties (*e.g.*, semiconducting,[30,31] ferroelectric,[32] superconducting,[33–35] and photo- and electrochromic properties).[36–39] Among them, the chromogenic effect discovered in amorphous and nanosized tungsten trioxides is of particular interest because these are promising candidates for industrial applications such as "smart windows" to control the input of solar light, glare control mirrors, and large area displays.[40,41] Realization of these properties in nanosheets would be intriguing because enhancement and some modulation of properties are expected due to the ultimately thin molecular structure. A nanosheet based on a tungsten oxide was recently synthesized by Schaak and Mallouk through delamination of a family of layered perovskites, $Bi_2W_2O_9$.[18] However, a follow-up study on its fundamental and practical aspects has not been reported presumably due to some difficulties in film fabrication. Therefore,

*Address correspondence to sasaki.takayoshi@nims.go.jp.

Received for review March 25, 2008 and accepted July 10, 2008.

Published online July 29, 2008.
10.1021/nn800184w CCC: $40.75

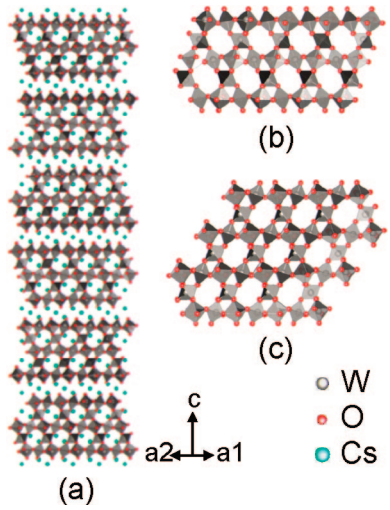

Figure 1. Crystal structure of $Cs_{6+x}W_{11}O_{36}$ viewed along the [110] direction, (a). Pyrochlore-type channels appeared in (b) the section view and in (c) the plane view (a 35° tilt from the horizontal alignment); Cs ions are omitted to highlight the channel structure.

exfoliation of other layered tungsten oxides is worth investigating.

The series of layered cesium tungstates is well-known for its framework called 2D pyrochlore structure (see Figure 1).[42–45] Typical modifications are identified as $Cs_{6+x}W_{11}O_{36}$ and $Cs_{8.5}W_{15}O_{48}$ that crystallize in a hexagonal structure. WO_6 octahedra are connected *via* corner-sharing to produce the 2D slab, in which interconnected channels, having the aperture of a six-membered ring, run in parallel to both the planar and axial directions. Cs ions are accommodated in the pyrochlore-type channels as well as the interlayer gallery. Although Cs ions are expected to have ion-exchange properties, few studies on their intercalation chemistry are reported in the literature. Such reactivity would be of great interest because soft-chemical modifications of the compound will be attained, offering possibilities for new or enhanced physicochemical properties. Furthermore, an intriguing single layer of 2D pyrochlore-type tungstate may be obtained *via* a delamination procedure typically induced by intercalation of bulky guests.

In the present study, we report the successful ion-exchange of the layered tungstate, $Cs_{6+x}W_{11}O_{36}$, into a protonated form and the subsequent exfoliation into 2D pyrochlore-related tungstate nanosheets. The unique structural features and chromogenic nature of the resulting nanosheets are described below.

RESULTS AND DISCUSSION

Ion-Exchange of Layered Cesium Tungstate. Synthesis at 1173 K produced a dark green sample, which was composed of densely gathered hexagonal plate-like single crystals. Powder X-ray diffraction (XRD) data of the ground sample can be indexed based on a hexagonal cell (see Figure 2a). The refined unit cell dimensions, $a = 0.7260(2)$ nm, $c = 11.083(3)$ nm, agree well with those reported for the layered cesium tungstate,[44,45] $Cs_{6+x}W_{11}O_{36}$. Chemical analysis revealed that the total value of cesium ions in the formula was 6.04 ± 0.04, indicating that the compound is almost stoichiometric in contrast to the previously reported material with $x = 0.31$. A slight excess of Cs ions leads to partial reduction of W^{6+} ions in the sample.[45] The presence of reduced tungsten ions may be responsible for sample coloration.

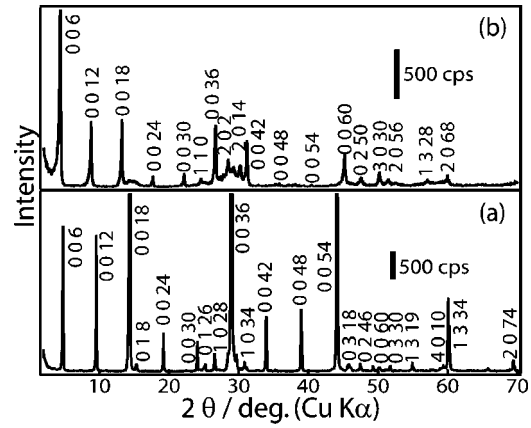

Figure 2. XRD patterns for (a) $Cs_{6+x}W_{11}O_{36}$ and (b) acid-exchanged form. All the peaks are indexed based on hexagonal structure.

When the $Cs_{6+x}W_{11}O_{36}$ powder was reacted with an HCl solution at various concentrations for 2 days, an obvious color change from dark green to white was observed at a concentration of 6 mol dm^{-3} and above (see Figure 3). The completely whitened sample displayed sharp XRD peaks (Figure 2b), which can be indexed based on the same hexagonal symmetry with the unit cell parameters of $a = 0.7254(2)$ nm, $c = 12.038(4)$ nm. The refined a parameter was very close to that of the $Cs_{6+x}W_{11}O_{36}$, suggesting that the 2D pyrochlore-type host layer was intact. In contrast, the c-axis parallel to the stacking direction became larger. This expansion most likely stems from the substitution of interlayer Cs ions with protons or oxonium ions. Judging from its color, the sample is believed to contain only oxidized

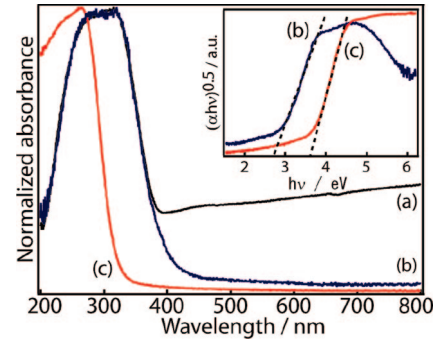

Figure 3. UV−vis diffuse reflectance spectra of (a) $Cs_{6+x}W_{11}O_{36}$, (b) acid-exchanged form and absorption spectrum of (c) nanosheet suspension. Inset shows the plot of $(\alpha h\nu)^{0.5}$ against $h\nu$ for samples (b) and (c).

tungsten ions, W^{6+}, meaning that the acid treatment brought about oxidative deintercalation of Cs ions in addition to normal ion-exchange reaction. In practice, evolution of H_2 gas was detected by gas chromatography when the acid treatment was carried out in a closed reaction vessel. This result should arise from the redox reaction between H^+ in the solution and the host oxide lattice, supporting this oxidation. On the basis of the chemical analysis, the acid-treated sample was formulated as $H_{2.10}Cs_{3.90}W_{11}O_{36} \cdot 6H_2O$.[46] The residual Cs ions in the formula should be located in the framework structure; the crystal structure data of $Cs_{6+x}W_{11}O_{36}$[44] indicate that the unit single host layer accommodates four Cs ions in its pyrochlore-type channels, giving an ideal chemical composition of $Cs_4W_{11}O_{36}{}^{2-}$. The other two Cs ions at the interlayer gallery are believed to be more easily extracted by the acid treatment than the inner Cs ions. As a result, the acid-exchanged product likely contains the protonic species in the interlayer gallery.

Exfoliation of the Protonated Cesium Tungstate into Single Host Layers. The protonated sample was reacted with aqueous solution containing tetrabutylammonium (TBA) ions equivalent to the ion-exchanged protons in the solid. A milky colloidal suspension was obtained after intermittent shaking for 10 days.

The dispersed material in the suspension could be totally sedimented by centrifugation at a speed of 10 000 rpm for 30 min. The sediment in wet state was subjected to XRD measurement at a relative humidity of 95% after being pasted to a sample holder. The pattern changed dramatically from that of the starting layered material to a broad and wavy profile. All sharp XRD peaks for the starting layered material were lost. Similar phenomena have been observed in other exfoliated nanosheet systems (*e.g.*, transition metal oxides[6,12,20] and layered double hydroxides).[23] The halo-like patterns were dependent on the layered materials and proved to be very similar to the square of the structure factor with the scattering vector normal to the sheet. This close match indicates that the host layers are no longer parallel at a constant separation, which can be taken as evidence of total delamination.

A structure factor $F(\theta)$ for the single host layer with a composition of $Cs_4W_{11}O_{36}$ is calculated to prove that this is true for the present case. As illustrated in Supporting Information S1, the host layer is centrosymmetric with respect to the horizontal plane at $z = 0$, thus $F(\theta)$ can be calculated by the following equation:

$$F(\theta) = \sum_i 2N_{W(i)}f_W\cos[2\pi\{2z_{W(i)}\sin\theta/\lambda\}] + \sum_i 2N_{Cs(i)}f_{Cs}\cos[2\pi\{2z_{Cs(i)}\sin\theta/\lambda\}] + \sum_i 2N_{O(i)}f_O\cos[2\pi\{2z_{O(i)}\sin\theta/\lambda\}] \quad (1)$$

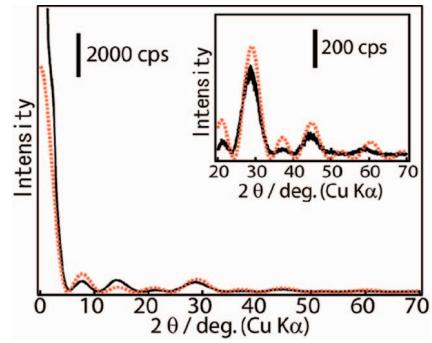

Figure 4. XRD profile for a colloidal sediment centrifuged from the suspension (solid line) and the square of the calculated structure factor for single cesium tungstate layer (broken line). The pattern was collected at a relative humidity of 95% to avoid undesirable drying.

where f_W, f_{Cs}, and f_O are the atomic scattering factors for W, Cs, and O atoms; $N_{W(i)}$, $N_{Cs(i)}$, and $N_{O(i)}$ are the number of *i*th W, Cs, and O atoms; and θ and λ are the diffraction angle and wavelength of the X-ray, respectively. The square of the calculated $F(\theta)$ designated as the broken line in Figure 4 can be reasonably fitted to the experimental data by changing the scale of the ordinate and taking into account the Lorentz polarization factor and the temperature factor.

Next, morphology of the cesium tungstate nanosheets was examined by means of transmission electron microscopy (TEM) observation. Figure 5 shows a typical image showing 2D sheets with faint but uniform contrast. Some of the sheets show evident triangular corners. The lateral size was several hundred nanometers for the nanosheet obtained by exfoliation with vigorous shaking at 180 rpm for 10 days. Note that gentler agitation yielded larger sheets of up to 100 μm. The selected area electron diffraction for the single nanosheet exhibited a single crystal-like pattern having sharp spots. These spots can be indexed in terms of a hexagonal unit cell of $a = 0.73$ nm, indicating that the pyrochlore-type 2D structure was maintained after delamination.

Characterization of the Cesium Tungstate Nanosheets in Unilamellar State. It is important to demonstrate film growth *via* electrostatic self-assembly using the newborn nanosheets not only for their application but also for understanding of their molecular entity. Actually,

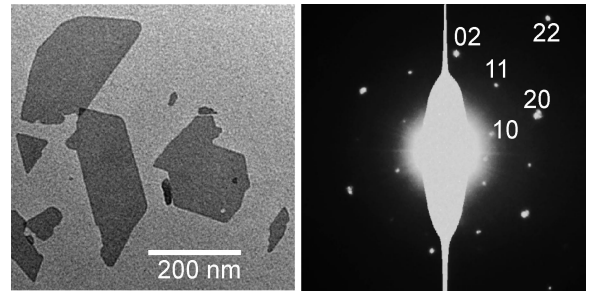

Figure 5. TEM micrograph of cesium tungstate nanosheets (left panel) and selected area electron diffraction pattern of single nanosheet (right panel).

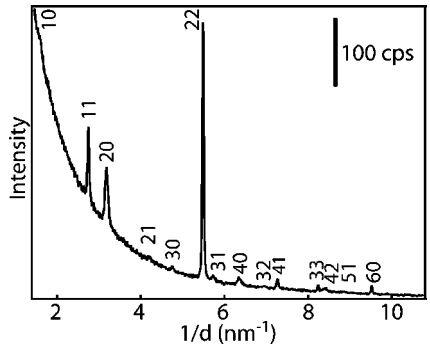

Figure 6. In-plane XRD pattern of the monolayer film of the nanosheets.

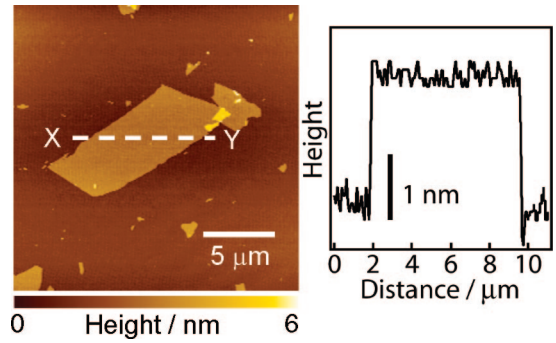

Figure 7. AFM image of cesium tungstate nanosheets on Si substrate. A height profile along the broken line from X to Y is shown in the right panel.

characterization of the self-assembled monolayer film of titania nanosheets[47,48] and manganese oxide nanosheets[20,49] has provided meaningful information on their structure in a unilamellar state. With respect to the tungsten oxide system, Schaak and Mallouk reported that the perovskite-type tungstate nanosheets, W_2O_7, were hardly adsorbed on the polycationic surface due to difficulty in displacing tetramethylammonium ions used as a delamination reagent.[18] Its exfoliation could not be achieved with larger TBA ions, which may be advantageous in self-assembly due to its lower charge density. In contrast, the present tungstate nanosheets, $Cs_4W_{11}O_{36}$, were obtained by exfoliation with TBA ions and were successfully adsorbed on a Si substrate coated with polycations. The monolayer film, in which the nanosheet lay flat to the substrate, was subjected to the following characterization.

In-plane XRD pattern for the monolayer film exhibited many sharp peaks in the 1/d region from 1.5 to 10.7 nm^{-1} (see Figure 6). All of the observable peaks are indexable to *hk* reflections of a 2D hexagonal cell, and its refined cell parameter was obtained as $a = 0.72695(3)$ nm. The resultant parameter correlates very closely with that of the bulk precursors. The characterizations suggest that the cesium tungstate nanosheets obtained in this study have interconnected pyrochlore-type channels. These channels have a diameter of about 0.53 nm between facing oxygen atoms across it and are comparable to zeolite cavities.[50]

Atomic force microscope (AFM) image of the nanosheet film displayed sheets showing sharp edges (Figure 7). Their average thickness was 2.2 ± 0.1 nm, and a lateral size was several tens of micrometers at the largest. The thickness is consistent with that of the host layer deduced from the crystallographic data for $Cs_{6+x}W_{11}O_{36}$; the vertical distance between the levels of upper and bottom oxygen atoms (O1 and O1′ in Supporting Information S1) of the host layer (1.55 nm) plus the ionic radius of these two oxygen atoms (0.28 nm) gives 1.83 nm.[44] This good agreement further supports the unilamellar nature of the obtained nanosheet crystallites. The difference between the experimental height and crystallographic thickness may be accounted for by adsorbed charge-compensating protons, oxonium ions, or water molecules, as is the case for other nanosheets.[20,47]

Optical Properties of the Cesium Tungstate Nanosheets. The colloidal suspension of the cesium tungstate nanosheets exhibited intense optical absorption at a wavelength of 350 nm and below, the absorbance of which was proportional to the concentration (see Supporting Information S2). The molar extinction coefficient for the chemical composition of $Cs_4W_{11}O_{36}$ was estimated to be 1.7×10^5 mol^{-1} dm^3 cm^{-1} at 260 nm. The square root of the absorption coefficient, α, times the photon energy, $h\nu$, for the nanosheet and the protonated precursor is plotted against the photon energy in Figure 3. The upsurge portions of $(\alpha h\nu)^{0.5}$ were well-fitted to a straight broken line, suggesting that the present tungstates have indirect electronic transition near the band gap. The optical band gap energy can be derived as about 3.6 eV for the nanosheets and 2.8 eV for the protonated precursor from the intersection of the broken line and the abscissa. The large difference of 0.8 eV may be explained by the size quantization effect arising from their nanoscale dimension. Similar energy increment incidental to the downsizing has been reported in hydrated WO_3 nanoparticles with a diameter of 5 nm and below.[38,51] For 2D anisotropic material including the nanosheet crystallites, the band gap shift is dominantly dependent on the sheet thickness.[52,53] Accordingly, the shift observed in the present tungstate nanosheets is likely explained by their thickness of much smaller than 5 nm. The cesium tungstate nanosheets can be described as a wide-gap semiconductor. The band gap energy is slightly smaller than that of titania nanosheets (3.84 eV),[53] which may be beneficial for photochemical applications.

Photochromism of the Cesium Tungstate Nanosheets. It is worth investigating color changes in cesium tungstate nanosheets upon light excitation because a related material of WO_3 is well-known for its photochromic behavior; the color can be reversibly switched by photoexcited electron−hole pair from transparent state to blue, associated with a broad absorption peak at 900−1000 nm.[36,37] We observed a reversible color change in re-

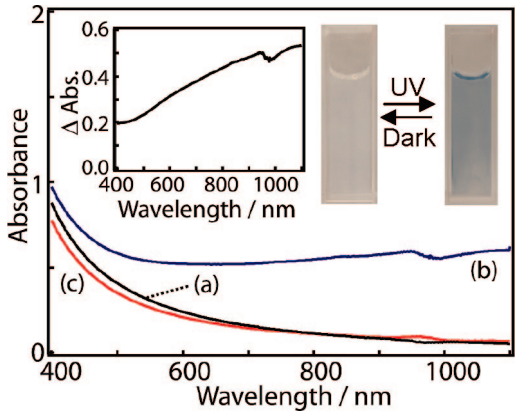

Figure 8. UV−vis spectra of the nanosheet suspension for (a) virgin, (b) colored, and (c) bleached states. Inset shows the difference in absorbance between colored and bleached states (left), and the nanosheet suspension in a 1 cm square cell (right).

sponse to on-and-off of UV irradiation for the colloidal nanosheet suspension of $Cs_4W_{11}O_{36}^{2-}$. UV−vis absorption spectra of the nanosheet suspension for virgin, coloration, and bleached states are displayed in Figure 8. As seen in the evolution of wide-ranging absorption, the transparent milky suspension turned visibly bluish black after UV irradiation for 30 min and saturated after 60 min. When the colored sample was stored under dark conditions, the color gradually bleached and eventually vanished (after 240 min under the present conditions), returning to the virgin state. The coloration/bleaching could be repeated at least several times, as confirmed in this experiment. The coloration behavior observed is comparable to that of hydrated WO_3.[36–39] Note that a small hump around 980 nm is attributable to vibration of the hydroxyl group in water warmed by the UV irradiation.

Absorbance gain estimated from the difference in absorbance between coloration and bleached states, ΔAbs, is an indicator of photochromic performance.[38,54,55] The ΔAbs for the nanosheet suspension with increasing wavelength reached to 0.5 at 940 nm under the present condition. A similar system of dispersed nanoparticles of $WO_3 \cdot 2H_2O$ in a 0.5 mm cell yielded ΔAbs of ~0.35 at a concentration of 0.31 mol dm^{-3}.[38] Although there is a difference in experimental conditions between the nanosheet and nanoparticle systems, simple comparison of ΔAbs normalized in terms of cell length and the number of W atom suggests that the tungstate nanosheet performance is at least six times better. A larger surface area enhances the coloration more effectively because adsorption of hydrogen molecules and charge-compensating cations to trapped electrons as a color center on the surface plays an important role in the coloration.[56–58] In view of this, the ultimate 2D structure of the nanosheets may be essential for the coloration performance, offering extensive sites for adsorbents.

The reversible color change revealed in this study definitely indicates that the cesium tungstate nanosheet exhibits photochromism in response to UV irradiation. Associated electrochromic properties should also be promising. Quantitative evaluation of photochromic performance, including sensitivity and reversibility and its mechanism for the nanosheet system, will be examined in a future study.

CONCLUSIONS

The 2D pyrochlore-type cesium tungstate of $Cs_{6+x}W_{11}O_{36}$ was converted into the protonated form of $H_{2.10}Cs_{3.90}W_{11}O_{36} \cdot 6H_2O$ through treatment with concentrated HCl solution. The interlayer protons were exchanged with bulky quaternary ammonium ions, which induced delamination into unilamellar colloidal sheets of $Cs_4W_{11}O_{36}^{2-}$ under optimal conditions. The resultant nanosheet crystallites possess interconnected pyrochlore-type channels, which may function as diffusion paths or adsorption sites for alkali metal ions, water, and small molecules. We demonstrated the efficient photochromic behavior of the cesium tungstate nanosheets, which is promising for constructing novel photo- and electrochromic materials or devices using chromogenic nanosheets as a building block.

EXPERIMENTAL SECTION

Material Synthesis. Layered cesium tungstate, $Cs_{6+x}W_{11}O_{36}$, was synthesized by heating a mixture of Cs_2CO_3 and WO_3 (4:11 molar ratio) at 1173 K for 5 h. The obtained single crystals were ground and then treated with HCl solution (1, 6, and 12 mol dm^{-3}) for 2 days at room temperature to promote proton exchange. The acid-treated sample (0.4 g) was immersed in 100 cm^3 of an aqueous solution containing 0.0028 mol dm^{-3} tetrabutylammonium hydroxide (TBAOH). Intermittent shaking for 10 days yielded a colloidal suspension with a milky appearance. A negligible amount of sediment was observed, implying nearly total delamination.

A Si wafer substrate was cleaned by dipping in HCl/CH_3OH (1:1) solution and then in concentrated H_2SO_4 solution. The hydrophilic substrate was immersed in an aqueous solution of poly(diallyldimethylammonium chloride) (pH = 9, 2.5 g dm^{-3}) for 20 min to precoat the surface. Then, it was dipped in a colloidal suspension of negatively charged nanosheets (pH = 8, 0.08 g dm^{-3}) for 20 min to fabricate a monolayer film, in which the nanosheets were adsorbed *via* self-assembly onto the substrate surface.

Measurements and Analysis. XRD data for powder and colloidal samples were collected by means of Bragg−Brentano-type diffractometers (Rigaku Rint 2000 and 2200HF, respectively) with Cu Kα radiation (λ = 0.15405 nm). The gaseous species evolved upon the acid treatment were identified by gas chromatography (Shimadzu GC-14, MS-5A column, Ar carrier). TEM study was performed with a JEOL 1010 transmission electron microscope operated at an accelerating voltage of 100 kV. Specimens were prepared by directly placing droplets of the colloidal nanosheet suspension onto a holey carbon coated Cu grid and removing the suspension after a while. In-plane XRD analysis on the monolayer film deposited on Si substrate was carried out with a four-axis diffractometer installed on the BL-6C at the Photon Factory

in the High Energy Accelerator Research Organization. The monochromated X-ray beam was focused on the incident slit by a cylindrical Pt mirror and struck the sample surface below the critical angle for total external reflection. The in-plane diffraction lines were recorded by NaI scintillation counter, the window of which is limited by a Soller slit (0.45°). A tapping-mode AFM (Seiko Instruments SPA400) with Si-tip cantilever (40 N m^{-1}) was used to evaluate the morphology of the obtained nanosheets on the Si substrate.

Optical absorption and diffuse reflectance spectra were recorded on a Hitachi U-4100 spectrophotometer equipped with an integration-sphere-type detector. Photochromism of the nanosheet suspension was assessed using a sealed single-compartment cell (5.5 cm thickness) with two quartz windows. The suspension was diluted to a concentration of 6.7×10^{-5} mol dm^{-3}, and its pH value was adjusted as ~5 with HCl solution. After the suspension was bubbled with N_2 gas, the cell was tightly sealed. A 500 W Xe lamp (XEF-501S, San-ei Electric) was used as the excitation source. Light intensity integrated from 200 to 500 nm was 14 mW cm^{-2}.

Chemical Analysis. A weighed amount (20 mg) of the sample was mixed with Na_2CO_3 (0.75 g) and H_3BO_3 (0.3 g) and was melted in a Pt crucible by heating. The cooled melt was dissolved with a mixed-acid solution of HCl (3 cm^3) and HF (1 cm^3). The obtained solution was diluted with ultrapure water (>18 MΩ · cm) and then subjected to quantitative analysis for Cs by atomic absorption spectrometry (Varian SpectrAA-20) and for W by inductively coupled plasma atomic emission spectrometry (Jarrell Ash IRIS Advantage). Weight loss up to 1273 K was measured by thermogravimetry (Rigaku Thermo Plus TG 8120) to estimate water content in the sample.

Acknowledgment. This work has been supported by CREST of the Japan Science and Technology Agency (JST), Japan Society for the Promotion of Sciences (JSPS), and World Premier International Research Center Initiative (WPI Initiative) on Materials Nanoarchitectonics, MEXT, Japan. Figure 1 was drawn with VENUS developed by R. A. Dilanian and F. Izumi (National Institute for Materials Science). The in-plane XRD measurements were performed with the approval of the Photon Factory Program Advisory Committee (2005G159).

Supporting Information Available: Figure S1 showing a side view of the single host layer, $Cs_4W_{11}O_{36}$, and its structural parameters. Figure S2 showing UV−vis absorption spectra obtained from the colloidal suspension of the cesium tungstate nanosheets with various concentrations. This material is available free of charge *via* the Internet at http://pubs.acs.org.

REFERENCES AND NOTES

1. Walker, G. F. Macroscopic Swelling of Vermiculite Crystals in Water. *Nature* **1960**, *187*, 312–313.
2. Nadeau, P. H.; Wilson, M. J.; McHardy, W. J.; Tait, J. M. Interstratified Clays as Fundamental Particles. *Science* **1984**, *225*, 923–925.
3. Leaf, A.; Schöllhorn, R. Solvation Reactions of Layered Ternary Sulfides A_xTiS_2, A_xNbS_2, and A_xTaS_2. *Inorg. Chem.* **1977**, *16*, 2950–2956.
4. Joensen, P.; Frindt, R. F.; Morrison, S. R. Single-Layer MoS_2. *Mater. Res. Bull.* **1986**, *21*, 457–461.
5. Yang, D.; Frindt, R. F. Li-Intercalation and Exfoliation of WS_2. *J. Phys. Chem. Solids* **1996**, *57*, 1113–1116.
6. Sasaki, T.; Watanabe, M.; Hashizume, H.; Yamada, H.; Nakazawa, H. Macromolecule-Like Aspects for a Colloidal Suspension of an Exfoliated Titanate. Pairwise Association of Nanosheets and Dynamic Reassembling Process Initiated from It. *J. Am. Chem. Soc.* **1996**, *118*, 8329–8335.
7. Sasaki, T.; Watanabe, M. Osmotic Swelling to Exfoliation. Exceptionally High Degrees of Hydration of a Layered Titanate. *J. Am. Chem. Soc.* **1998**, *120*, 4682–4689.
8. Sugimoto, W.; Terabayashi, O.; Murakami, Y.; Takasu, Y. Electrophoretic Deposition of Negatively Charged Tetratitanate Nanosheets and Transformation into Preferentially Oriented TiO_2(B) Film. *J. Mater. Chem.* **2002**, *12*, 3814–3818.
9. Miyamoto, N.; Kuroda, K.; Ogawa, M. Exfoliation and Film Preparation of a Layered Titanate, $Na_2Ti_3O_7$, and Intercalation of Pseudoisocyanine Dye. *J. Mater. Chem.* **2004**, *14*, 165–170.
10. Treacy, M. M. J.; Rice, S. B.; Jacobson, A. J.; Lewandowski, J. T. Electron Microscopy Study of Delamination in Dispersions of the Perovskite-Related Layered Phases $K[Ca_2Na_{n-3}Nb_nO_{3n-1}]$: Evidence for Single-Layer Formation. *Chem. Mater.* **1990**, *2*, 279–286.
11. Schaak, R. E.; Mallouk, T. E. Perovskites by Design: A Toolbox of Solid-State Reactions. *Chem. Mater.* **2002**, *14*, 1455–1471.
12. Ebina, Y.; Sasaki, T.; Watanabe, M. Study on Exfoliation of Layered Perovskite-Type Niobates. *Solid State Ionics* **2002**, *151*, 177–182.
13. Takagaki, A.; Lu, D.; Kondo, J. N.; Hara, M.; Hayashi, S.; Domen, K. Exfoliated HNb_3O_8 Nanosheets as a Strong Protonic Solid Acid. *Chem. Mater.* **2005**, *17*, 2487–2489.
14. Miyamoto, N.; Yamamoto, H.; Kaito, R.; Kuroda, K. Formation of Extraordinarily Large Nanosheets from $K_4Nb_6O_{17}$ Crystals. *Chem. Commun.* **2002**, 2378–2379.
15. Schaak, R. E.; Mallouk, T. E. Prying Apart Ruddlesden-Popper Phases: Exfoliation into Sheets and Nanotubes for Assembly of Perovskite Thin Films. *Chem. Mater.* **2000**, *12*, 3427–3434.
16. Takagaki, A.; Yoshida, T.; Lu, D.; Kondo, J. N.; Hara, M.; Domen, K.; Hayashi, S. Titanium Niobate and Titanium Tantalate Nanosheets as Strong Solid Acid Catalysts. *J. Phys. Chem. B* **2004**, *108*, 11549–11555.
17. Fukuda, K.; Nakai, I.; Ebina, Y.; Ma, R.; Sasaki, T. Colloidal Unilamellar Layers of Tantalum Oxide with Open Channels. *Inorg. Chem.* **2007**, *46*, 4787–4789.
18. Shaack, R. E.; Mallouk, T. E. Exfoliation of Layered Rutile and Perovskite Tungstates. *Chem. Commun.* **2002**, 706–707.
19. Liu, Z.-H.; Ooi, K.; Kanoh, H.; Tang, W.-P.; Tomida, T. Swelling and Delamination Behaviors of Birnessite-Type Manganese Oxide by Intercalation of Tetraalkylammonium Ions. *Langmuir* **2000**, *16*, 4154–4164.
20. Omomo, Y.; Sasaki, T.; Wang, L. Z.; Watanabe, M. Redoxable Nanosheet Crystallites of MnO_2 Derived *via* Delamination of a Layered Manganese Oxide. *J. Am. Chem. Soc.* **2003**, *125*, 3568–3575.
21. Adachi-Pagano, M.; Forano, C.; Besse, J. Delamination of Layered Double Hydroxides by Use of Surfactants. *Chem. Commun.* **2000**, 91–92.
22. Hibino, T.; Jones, W. New Approach to the Delamination of Layered Double Hydroxides. *J. Mater. Chem.* **2001**, *11*, 1321–1323.
23. Li, L.; Ma, R.; Ebina, Y.; Iyi, N.; Sasaki, T. Positively Charged Nanosheets Derived *via* Total Delamination of Layered Double Hydroxides. *Chem. Mater.* **2005**, *17*, 4386–4391.
24. Liu, Z.; Ma, R.; Ebina, Y.; Iyi, N.; Takada, K.; Sasaki, T. General Synthesis and Delamination of Highly Crystalline Transition-Metal-Bearing Layered Double Hydroxides. *Langmuir* **2007**, *23*, 861–867.
25. Kleinfeld, E. R.; Ferguson, G. S. Stepwise Formation of Multilayered Nanostructural Films from Macromolecular Precursors. *Science* **1994**, *265*, 370–373.
26. Kaschak, D. M.; Lean, J. T.; Waraksa, C. C.; Saupe, G. B.; Usami, H.; Mallouk, T. E. Photoinduced Energy and Electron Transfer Reactions in Lamellar Polyanion/Polycation Thin Films: Toward an Inorganic "Leaf". *J. Am. Chem. Soc.* **1999**, *121*, 3435–3445.
27. Sasaki, T.; Ebina, Y.; Watanabe, M.; Decher, G. Multilayer Ultrathin Films of Molecular Titania Nanosheets Showing Highly Efficient UV-Light Absorption. *Chem. Commun.* **2000**, 2163–2164.
28. Wang, Z.-S.; Sasaki, T.; Muramatsu, M.; Ebina, Y.; Tanaka, T.; Wang, L.-Z.; Watanabe, M. Self-Assembled Multilayers of Titania Nanoparticles and Nanosheets with Polyelectrolytes. *Chem. Mater.* **2003**, *15*, 807–812.
29. Li, L.; Ma, R.; Ebina, Y.; Fukuda, K.; Takada, K.; Sasaki, T. Layer-by-Layer Assembly and Spontaneous Flocculation of Oppositely Charged Oxide and Hydroxide Nanosheets into

Inorganic Sandwich Layered Materials. *J. Am. Chem. Soc.* **2007**, *129*, 8000–8007.
30. Giraudeau, A; Fan, F.-R. F; Bard, A. J. Spectral Sensitization of the Semiconductors Titanium Oxide (n-TiO_2) and Tungsten Oxide (n-WO_3) with Metal Phthalocyanines. *J. Am. Chem. Soc.* **1980**, *102*, 5137–5142.
31. Nenadovic, M. T.; Rajh, T.; Micic, O. I.; Nozik, A. J. Electron Transfer Reactions and Flat-Band Potentials of Tungsten(VI) Oxide Colloids. *J. Phys. Chem.* **1984**, *88*, 5827–5830.
32. Subbarao, E. C. Ferroelectric and Antiferroelectric Materials. *Ferroelectrics* **1973**, *5*, 267–280.
33. Stanley, R. K.; Morris, R. C.; Moulton, W. G. Conduction Properties of the Hexagonal Tungsten Bronze, Rb_xWO_3. *Phys. Rev. B* **1979**, *20*, 1903–1914.
34. Skokan, M. R.; Moulton, W. G.; Morris, R. C. Normal and Superconducting Properties of Cs_xWO_3. *Phys. Rev. B* **1979**, *20*, 3670–3677.
35. Cadwell, L. H.; Morris, R. C.; Moulton, W. G. Normal and Superconducting Properties of K_xWO_3. *Phys. Rev. B* **1981**, *23*, 2219–2223.
36. Deb, S. K. Optical and Photoelectric Properties and Color Centers in Thin-Films of Tungsten Oxide. *Philos. Mag.* **1973**, *27*, 801–822.
37. Shigesato, Y. Photochromic Properties of Amorphous WO_3 Films. *Jpn. J. Appl. Phys* **1991**, *30*, 1457–1462.
38. Bedja, I.; Hotchandani, S.; Kamat, P. V. Photoelectrochemistry of Quantized Tungsten Trioxide Colloids: Electron Storage, Electrochromic, and Photoelectrochromic Effects. *J. Phys. Chem.* **1993**, *97*, 11064–11070.
39. Bedja, I.; Hotchandani, S.; Carpentier, R.; Vinodgopal, K.; Kamat, P. V. Electrochromic and Photoelectrochemical Behavior of Thin WO_3 Films Prepared from Quantized Colloidal Particles. *Thin Solid Films* **1994**, *247*, 195–200.
40. Bange, K.; Gambke, T. Electrochromic Materials for Optical Switching Devices. *Adv. Mater.* **1990**, *2*, 10–16.
41. Rubin, M. Ion-Assisted Sputtering of Tungsten Oxide Solar-Control Films. *J. Vac. Sci. Technol. A* **1992**, *10*, 1905–1907.
42. Okada, K.; Marumo, F.; Iwai, S. The Crystal Structure of $Cs_6W_{11}O_{36}$. *Acta Crystallogr.* **1978**, *B34*, 50–54.
43. Kudo, T.; Oi, J.; Kishimoto, A.; Hiratani, M. Three Kinds of Framework Structures of Corner-Sharing WO_6 Octahedra Derived from Peroxo-Polytungstates as a Precursor. *Mater. Res. Bull.* **1991**, *26*, 779–787.
44. Marsh, R.; Bernal, I. More Space-Group Changes. *Acta Crystallogr.* **1995**, *B51*, 300–307.
45. Solodovnikov, S. F.; Ivannikova, N. V.; Solodovnikova, Z. A.; Zolotova, E. S. Synthesis and X-Ray Diffraction Study of Potassium, Rubidium, and Cesium Polytungstates with Defect Pyrochlore and Hexagonal Tungsten Bronze Structures. *Inorg. Mater.* **1998**, *34*, 845–853.
46. Standard deviation of the Cs content was 0.03.
47. Sasaki, T.; Ebina, Y.; Kitami, Y.; Watanabe, M.; Oikawa, T. Two-Dimensional Diffraction of Molecular Nanosheet Crystallites of Titanium Oxide. *J. Phys. Chem. B* **2001**, *105*, 6116–6121.
48. Fukuda, K.; Nakai, I.; Oishi, C.; Nomura, M.; Harada, M.; Ebina, Y.; Sasaki, T. Nanoarchitecture of Semiconductor Titania Nanosheets Revealed by Polarization-Dependent Total Reflection Fluorescence X-ray Absorption Fine Structure. *J. Phys. Chem. B* **2004**, *108*, 13088–13092.
49. Fukuda, K.; Nakai, I.; Ebina, Y.; Tanaka, T.; Mori, T.; Sasaki, T. Structure Analysis of Exfoliated Unilamellar Crystallites of Manganese Oxide Nanosheets. *J. Phys. Chem. B* **2006**, *110*, 17070–17075.
50. Ribeiro, F. R.; Rodrigues A. E.; Rollmann, L. D.; Naccache, C. *Zeolites: Science and Technology*; Martinus Nijhoff Publishers: The Hague, Boston, Lancaster, 1984.
51. He, Y.; Wu, Z.; Fu, L.; Li, C.; Miao, Y.; Cao, L.; Fan, H.; Zou, B. Photochromism and Size Effect of WO_3 and WO_3-TiO_2 Aqueous Sol. *Chem. Mater.* **2003**, *15*, 4039–4045.
52. Sasaki, T.; Watanabe, M. Semiconductor Nanosheet Crystallites of Quasi-TiO_2 and Their Optical Properties. *J. Phys. Chem. B* **1997**, *101*, 10159–10161.
53. Sakai, N.; Ebina, Y.; Takada, K.; Sasaki, T. Electronic Band Structure of Titania Semiconductor Nanosheets Revealed by Electrochemical and Photoelectrochemical Studies. *J. Am. Chem. Soc.* **2004**, *126*, 5851–5858.
54. He, T.; Ma, Y.; Cao, Y.; Hu, X.; Liu, H.; Zhang, G.; Yang, W.-S.; Yao, J.-N. Photochromism of WO_3 Colloids Combined with TiO_2 Nanoparticles. *J. Phys. Chem. B* **2002**, *106*, 12670–12676.
55. Avellaneda, C. O.; Bulhões, L. O. S. Photochromic Properties of WO_3 and WO_3:X (X = Ti, Nb, Ta and Zr) Thin Film. *Solid State Ionics* **2003**, *165*, 117–121.
56. Bechinger, C.; Oefinger, G.; Herminghaus, S.; Leiderer, P. On the Fundamental Role of Oxygen for the Photochromic Effect of WO_3. *J. Appl. Phys.* **1993**, *74*, 4527–4533.
57. Zhang, J.-G.; Benson, D. K.; Tracy, C. E.; Deb, S. K.; Czanderna, A. W.; Bechinger, C. Chromic Mechanism in Amorphous WO_3 Films. *J. Electrochem. Soc.* **1997**, *144*, 2022–2026.
58. He, T.; Ma, Y.; Cao, Y.; Yang, W.-S.; Yao, J.-N. Improved Photochromism of WO_3 Thin Films by Addition of Au Nanoparticles. *Phys. Chem. Chem. Phys.* **2002**, *4*, 1637–1639.